JMEPEG (2004) 13:406-412
DOI: 10.1361/10599490419919

1059-9495/$19.00

Microstructure and Properties of TiB/Ti-6Al-4V Coatings Produced With Laser Treatments

D. Galvan, V. Ocelík, Y. Pei, B.J. Kooi, Jeff Th.M. De Hosson, and E. Ramous

(Submitted February 10, 2004)

TiB/Ti-6Al-4V metal-matrix composite (MMC) layers were produced on Ti-6Al-4V substrates by laser cladding. A TiB_2/Ti powder mixture was used as a precursor to obtain a dispersion of TiB needles in the Ti alloy matrix, with the aid of an exothermic reaction between TiB_2 and Ti. A eutectic microstructure was obtained that consisted of an extremely homogeneous dispersion of TiB eutectic needles in the Ti alloy matrix, having a volume fraction as high as 0.33. Also, an equilibrium-like microstructure was found, consisting of a dispersion of both primary and eutectic TiB needles inside the Ti alloy matrix. An analysis of the geometry of the layers was performed and proved successful in determining the percentage of B. Further, it correctly predicted the variation of atomic B content as a function of laser power. The relative wear resistance coefficient, defined as the wear coefficient of the uncoated matrix divided by that of coating, shows an improvement by a factor as high as 1500 for the eutectic microstructure.

Keyword laser processing, microstructure, TiB coatings, wear properties

1. Introduction

Despite the attractive properties of Ti alloys, e.g., high specific mechanical strength, high melting temperature, and good corrosion resistance, their tribological properties are rather poor.[1] This limits the use of uncoated Ti alloys to applications with low contact loads. Titanium has already been shown to be a suitable substrate for laser surface modification techniques, such as laser melt injection, leading to the formation of a wear-resistant metal-matrix composite (MMC) layer on top of the substrate.[2-4] TiB/Ti MMCs have already been synthesized in bulk form,[5,6] and surface layers of this composite have been obtained through high-energy electron beam irradiation,[7] laser cladding,[8] and solid-state diffusion.[9] This paper concentrates on tailoring the microstructure of a TiB/Ti-6Al-4V MMC coating for tribological applications. The technique of laser cladding has been scrutinized, and a systematic analysis of the processing parameters is presented. A MMC layer is formed in situ through the reaction between TiB_2 particles injected in a laser-induced melt pool and the surrounding Ti of the substrate. This results in the formation of TiB needles through an exothermic reaction.[10] The phase diagram of the Ti-B system can be found in Ref 1, and various phases may exist, namely TiB, TiB_2, and Ti_3B_4, together with α- and β-Ti. In particular, the eutectic point at 7 at.% B and 1540 °C is relevant for our work. The chemical reaction leading to the formation of the composite follows the reaction $TiB_2 + Ti \rightarrow 2TiB$. The thermodynamics of the reaction has been further analyzed by Zhang et al.[10] Both the change of Gibbs free energy and enthalpy are negative.

In in situ MMCs,[11] the reinforcements are synthesized in the metallic matrix by chemical reactions between elements or compounds during the composite fabrication. They exhibit a range of advantages, as compared with conventional MMCs: They can exhibit better behavior in high-temperature service conditions, as the reinforcing phase will be thermodynamically stable inside the matrix. Also, the reinforcement-matrix interfaces will be clean and, therefore, more resistant. Finally, the in situ formed reinforcing phase will have finer dimensions, and it will be more homogeneously distributed inside the matrix. This latter advantage is particularly relevant because with the laser melt injection technique, the diameter of the powder cannot be smaller than about 30 μm due to problems with particle feeding and penetration in the melt pool.[12]

2. Experiments

The experimental setup for laser cladding consists of a Rofin-Sinar (Hamburg, Germany) Nd:YAG 2 kW laser (λ = 1.06 μm), and a CNC table with which it is possible to move the substrate underneath the beam with a controllable speed. The laser beam is transported by means of a 0.8 mm diameter optical fiber. After leaving the fiber, the beam is collimated and focused through a water-cooled lens system with a focal length of 120 mm. The laser beam departs from a nozzle through which He gas is used to shield the lens and prevent oxidation and nitriding of the specimen by air. The dimensions of the Ti-6Al-4V substrate in this experiment were 150 × 100 × 5 mm.

Two different powders were fed into the melt pool of the substrate through two Metco 9PM (Wohlen, Switzerland) powder-feeding apparatus. The powders were injected into a cyclone where they were mixed together, and which partially

This paper was presented at the 2nd International Surface Engineering Congress sponsored by ASM International, on September 15-17, 2003, in Indianapolis, Indiana, and appeared on pp. 411-18 of the Proceedings.

D. Galvan, V. Ocelík, Y. Pei, B.J. Kooi, and **Jeff Th.M. De Hosson,** Department of Applied Physics, Materials Science Center and the Netherlands Institute for Metals Research, Nijenborgh 4, 9747 Ag Groningen, The Netherlands; and **E. Ramous,** DIMEG, Università di Padova, 35131 Padova, Italy. Contact e-mail: J.T.M.de.Hosson@phys.rug.nl.

separated the carrier gas from the particle stream due to gravity. This resulted in a slower stream of particles. The particle stream flowing out from a ∅ 2 mm nozzle hit the substrate at an angle of 47° with respect to the surface normal. The powders consisted of TiB_2 particles with a size range between 5 and 25 μm, as well as Ti particles having a size of 90 ± 22 μm. A heating plate was used to preheat the substrate as needed.

The following processing window has been investigated: scanning speed 150-500 mm/min, laser power density 130-240 W/mm^2, laser power 800-1500 W, carrier gas 2-7 L/min Ar, shielding gas 2-5 L/min He, powder feed rate 0-1.5 g/min, weight ratio of the precursor powders (TiB_2:Ti) 1/2-2/1, and substrate preheat temperature (20 and 300 °C).

Cross sections of the tracks were cut, embedded in Demotec plastic and lightly etched with Weck's reagent [100 mm^3 H_2O, 5 g ammonium bifluoride]. The samples were observed with an optical microscope, followed by electron microscopy observations (Philips XL30 FEG SEM) (Acht, The Netherlands). In situ tensile tests were carried out in an environmental scanning electron microscope (SEM; Philips XL30 FEG E-SEM). Nanoindentations were performed using an MTS Nano Indenter XP (Eden Prairie, MN) employing the so-called continuous stiffness measurement technique (CSM)[13] with a Berkovich tip. Samples for wear tests were cut from 5 mm thick substrates by spark erosion with dimensions of 10 × 5 × 2 mm. Wear tests were performed using a Plint TE67 (Newbury, UK) tribometer using the pin-on-disk set up. Stationary specimens were pressed with a known normal force against the surface of a rotating 100Cr6 hardened (60 HRc) steel disk, with an initial surface roughness of R_a = 0.1 μm. Specimen and disk were completely submerged in an oil bath (B.P. Transcal N, Southampton, UK), and the test was performed at room temperature. To exclude hydrodynamic lift effects, and to perform the wear test under boundary lubrication conditions, wear experiments were performed at a low constant sliding speed (0.01 m/s) for contact pressures of 20 and 100 MPa. Before and after the wear test, the samples were weighed to determine the mass loss. A single circle x-ray diffractometer (Philips PW-1830) was used to identify the phases present within the layers using Cu K_α radiation. The volume fraction of TiB has been measured directly using image analysis software applied to optical micrographs. The atomic percentage of B in the layers is related to the V_F of TiB according to

$$B\% = \left\{ \frac{\left(\frac{\rho_{TiB}}{M(TiB)}\right) \cdot V_F}{2 \cdot \left(\frac{\rho_{TiB}}{M(TiB)}\right) \cdot V_F + \left(\frac{\rho_{Ti}}{M(Ti)}\right) \cdot (1 - V_F)} \right\} \cdot 100 \quad \text{(Eq 1)}$$

where ρ is the density of the indicated material (4.56 and 4.50 g/cm^3 for TiB and Ti, respectively[1,14]) and M is its atomic weight.

3. Results

A typical cross section of a laser track is depicted in Fig. 1. Noteworthy is the asymmetric shape of the melt pool, which is deeper at the point highlighted by an arrow. At this point, a partially reacted TiB_2 particle is present, with the TiB reaction products visible. It was observed that the lower the laser scanning speed, the lower the content of unreacted TiB_2 particles inside the layers. A low scanning speed of 200 mm/min was therefore chosen. Successive steps were aimed at increasing the volume fraction of TiB to the maximum extent with the needles remaining separated from each other, so that the area of interface between the composite matrix and the TiB needles is maximized.

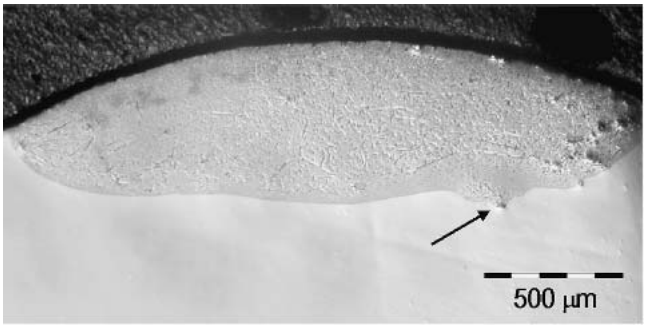

Fig. 1 Optical micrograph of the cross section of a laser track. Residual TiB_2 particles present only on the top and on the right side of the track. An arrow indicates a partially reacted TiB_2 particle.

A higher laser power proved to result in a larger dissolution of TiB_2 precursor. The amount of injected TiB_2 powder and, consequently, the applied laser power were increased. A typical microstructure of layers obtained with larger quantities of TiB_2 precursor and with a higher laser power is displayed in Fig. 2. The TiB needles formed are not uniformly distributed in the matrix, but instead they exist only in the interdendritic area as a eutectic phase.

The fraction of B in this layer equals 0.2, corresponding to a B atomic percentage of 15. For the track whose microstructure is depicted in Fig. 2, "frozen" vortices resulting from Marangoni flows[15] were observed. This structure is typical of high cooling rate solidification and it is not homogeneous. Therefore, it is thought not to be suitable for tribological applications. A substrate preheat of 300 °C was used to reduce the cooling rate, and eight tracks were obtained by varying the applied laser power and the amount of injected powder.

In Fig. 3, the microstructure of the layer obtained at 1000 W for the higher amount of injected powder is displayed. It contains both primary and eutectic TiB needles and exhibits a V_F of TiB of 0.40. This corresponds to a 26 at.% of B. The observed microstructure is expected from the phase diagram at the measured at.% B. Noteworthy in Fig. 3 are the primary TiB needles surrounded by a halo of Ti. The eutectic needles are absent. In Fig. 4 and 5, the microstructures of the layers obtained with the highest laser power (1400 W) are shown, with injected powder containing 0.7 g/min TiB_2 plus 0.3 g/min Ti. Noteworthy are the total lack of primary TiB needles and the occurrence of the structure at different amounts of injected powders, with volume fractions that logically vary as a function of the amount of added powder, being 0.27 and 0.33, respectively. These volume fractions correspond to a B at.% of 19 and 22. The x-ray diffraction (XRD) measurements show similar results; i.e., all the phases listed in the phase diagram were detected, namely α-Ti, β-Ti, Ti_3B_4, TiB_2, and TiB.

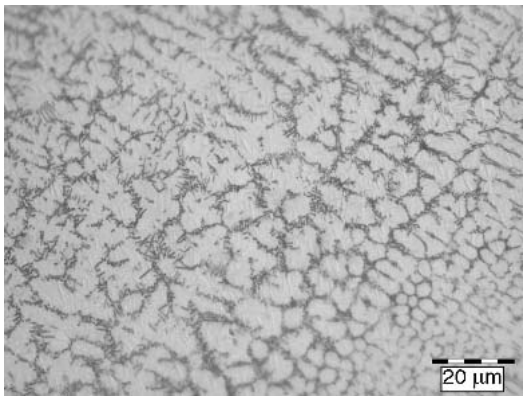

Fig. 2 Optical micrograph of a dendritic microstructure (1000 W laser power, scanning speed 200 mm/min, and powder feed rate 1 g/min TiB_2 plus 0.5 g/min Ti). The volume fraction V_F of TiB in the clad layer is about 0.20, corresponding to 15 at.% B.

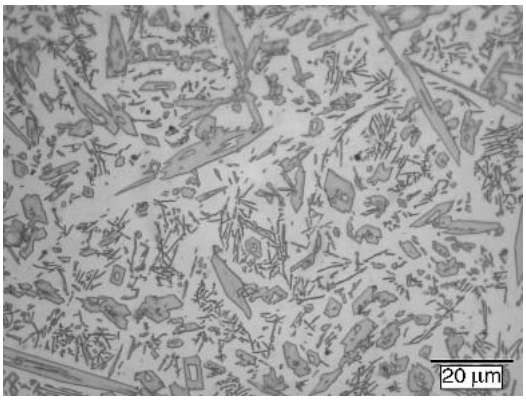

Fig. 3 Optical micrograph of primary TiB microstructure (1000 W laser power, scanning speed 200 mm/min, powder feed rate 1 g/min TiB_2 + 0.5 g/min Ti, and preheating of the substrate to 300 °C applied). The V_F of TiB in the clad layer is about 0.40, i.e., 26 at.% B.

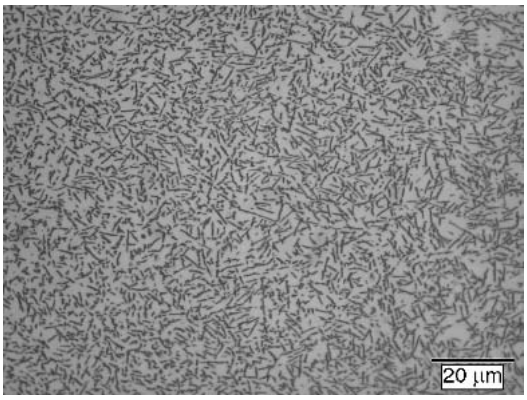

Fig. 4 Optical micrograph of a eutectic microstructure (1400 W laser power, scanning speed 200 mm/min, powder feed rate 0.7 g/min TiB_2 + 0.3 g/min Ti, and preheating of the substrate to 300 °C applied). The V_F of TiB in the clad layer is about 0.27, corresponding to 19 at.% B.

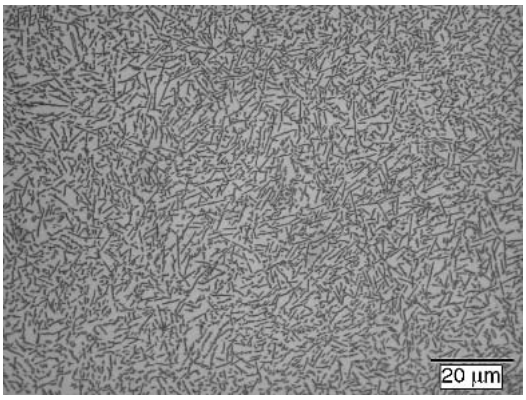

Fig. 5 Optical micrograph of eutectic microstructure (1400 W laser power, scanning speed 200 mm/min, powder feed rate 1 g/min TiB_2 + 0.5 g/min Ti, and preheating of the substrate to 300 °C). The V_F of TiB in the clad layer is about 0.33, corresponding to 22 at.% B.

Nanoindentations were performed on polished cross sections of the tracks. In one case, the indentations were directed toward the primary TiB needles, and the CSM technique was used. A maximum load of 20 mN was selected, and the indentations were successfully accomplished while monitoring the hardness as the indenter penetrated the material. Parts of the hardness curves were subsequently selected as representative of the material hardness, and the values were averaged to give a value of 30.7 ± 1.1 GPa for the hardness of the TiB primary needles. The Young's modulus of the needles was also measured using the CSM technique, setting Poisson's ratio $\nu = 0.16$, as indicated in literature.[16] The value obtained was $E = 519 \pm 30$ GPa, which is comparable to the value of 482 GPa,[17] derived from the elastic response of an analogous MMC using a Halphin-Tsai equation approach.[18]

A hardness profile was obtained for the eutectic layer (Fig. 6). For these nanoindentations, the values of hardness were calculated from the unloading part of the curve (standard procedure), so that the highest possible amount of material was probed while maintaining high lateral resolution. Groups of four indentations were performed up to a maximum load of 30 mN for each value of depth. The values obtained for the hardness were averaged for each depth, and the error was estimated from the standard deviation of the four values. The hardness of the layer (about 7.5 GPa) is considerably higher than that of the substrate ($H_{Ti\text{-}6Al\text{-}4V} = 1.2$ GPa, from Ref 1). The hardness is constant throughout the layer and the transition is very abrupt from the layer to the heat-affected zone (HAZ), i.e., about 4 GPa.

A rule-of-mixture (ROM) calculation for the overall hardness of the composite yields 12 and 5.4 GPa as upper and lower limits. The uncertainty in these values is due to the approximate method of evaluation of the volume fraction of TiB phase (approximated to 0.3). The procedure to calculate the higher and lower limit is explained in Ref 19. With respect to the Voigt model,[18] the two limiting values correspond to the case where equal strain or equal stress is assumed in the TiB phase and the matrix, respectively. The case of equal strain corresponds to the situation when the deformation is totally transferred through the interface, i.e., when the interface is strong. The case of equal stress corresponds to the situation when the interface is weak, and in this case, the (hard) phase does not affect the deformation of the matrix. By comparing the hardness value with the higher and lower ROM bound values, it is

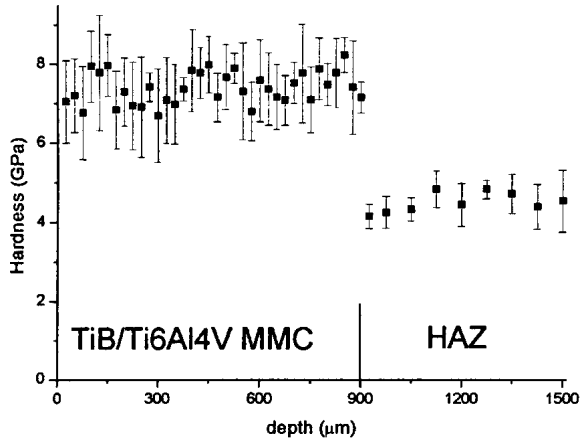

Fig. 6 Hardness profile of the eutectic track. The hardness of each point results from averaging four values obtained at that depth; the error is represented by the standard deviation.

possible to assess the quality of the interface, depending on which calculated bound is closer to the measured one. In our case the ROM value points at a strong interface.

In situ tensile tests were performed and proved that a strong interface existed with the Ti matrix for both the primary and the eutectic needles. In fact, delamination was never observed for the eutectic needles and only in one case was it observed for primary needles. In Fig. 7, a primary TiB needle is shown that has partly delaminated from the matrix, but this occurred during fracture of the needle; i.e., the TiB primary needle had already served its purpose, bearing the load until fracture.

Table 1 summarizes the results of all the wear tests. For the sake of comparison, the same wear tests were performed on untreated Ti-6Al-4V and the alloy remelted with a laser beam. Due to very intensive wear, the tests for the untreated and the laser remelted Ti-6Al-4V substrates were aborted after 3 and 4 h, respectively. They were performed for the lower applied pressure only (20 MPa). The value of specific wear rate (k_w) was determined from pin mass loss measured by weighing it before and after the test, using known densities of the substrate alloy and particles, and taking into account the volume fraction of ceramic particles in the coating. Benefits of reduced wear in laser coatings can be described by the "relative wear resistance" (RWR). It is defined as the wear coefficient of the uncoated matrix divided by that of coating.[20] The values of this coefficient for the present coatings are about 5, 400, and 1500 for the laser melted base alloy, the primary microstructure, and the eutectic microstructure, respectively.

3. Discussion

The temperature reached inside the melt pool was not monitored during laser cladding, but it can be inferred that it is between the melting point of TiB (2190 °C[14]) and the boiling point of Ti (3287 °C[1]). Indeed, if this latter temperature had been reached, substantial changes in the layer morphology would have occurred, and this has never been observed. Figure 3 shows that the melt pool has been melted to a deeper point, corresponding to a residual TiB_2 particle. Actually, it is evi-

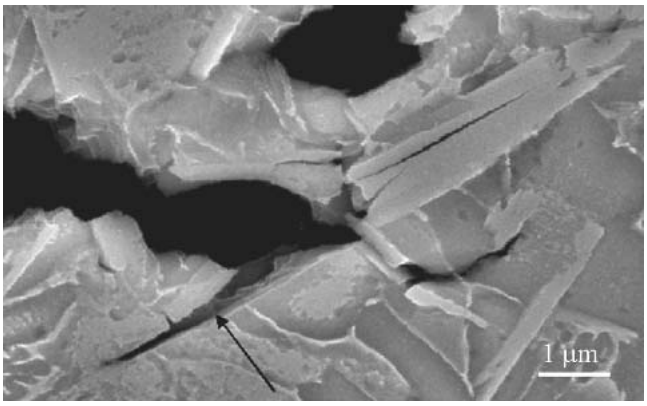

Fig. 7 SEM image of a primary TiB needle obtained during the in situ tensile test. An arrow indicates cracking of the needle and delamination.

Table 1 Wear Rate k_w [10^{-6} mm^3/Nm] Measured by the Pin-on-Disk Test

Microstructure	Contact Stress, MPa	k_w, 10^{-6} mm^3/Nm
Ti-6Al-4V substrate	20	189
Laser remelted Ti-6Al-4V	20	40
Coating: primary TiB	20	0.436
	100	0.483
Coating: eutectic TiB	20	0.125
	100	0.128

dence of the exothermic chemical reaction between Ti and TiB_2, namely: $TiB_2 + Ti \rightarrow TiB$ with the exothermic heat ΔH equal to −45 kJ/mol (at 2300 °C[10]). The heat of fusion for pure Ti is equal to 15.45 kJ/mol. Therefore, almost 3 mol Ti can be melted due to the chemical reaction between 1 mol Ti and 1 mol TiB_2. The dissolution of the TiB_2 particles after injection in the laser pool is best seen as a reactive decomposition, and it was observed to a larger extent at lower scanning speed and higher laser power.

The scanning speed of the laser is directly related to the lifetime of the melt pool. The use of higher laser power resulted in a higher temperature, both for the particles entering the melt pool and of the melt pool itself, thereby increasing its lifetime. When the parameters are such that the lifetime of the melt pool is long enough for the reaction to take place, the exothermic heat enhances the lifetime of the melt pool further. Eventually it causes the complete dissolution of the injected particles and results in a homogeneous microstructure. The enhanced homogeneity of the layer is due to the evolution of convective flows (Marangoni flows) inside the melt pool. These flows redistribute the material inside the melt pool and contribute to the homogeneity of the layer, if the lifetime of the melt pool is long enough.

The B content of all samples is higher than the eutectic concentration, i.e., 7%, corresponding to V_F of 0.09. The equilibrium microstructure should then consist of primary TiB needles and Ti/TiB eutectic. This is not always observed (Fig. 3 and 4), and it must be emphasized that laser processing is not an equilibrium processing technique. Therefore, inspection of the phase diagram may lead to erroneous predictions

due to the kinetic constraints involved. The eutectic microstructures shown in Fig. 4 have an atomic percent B (as estimated by the measurement of the V_F) that is considerably higher than the theoretical eutectic one. Therefore, solidification occurs within a "coupled zone." This zone is the range of alloy composition and growth rate where it is possible to solidify hypereutectic melts as eutectic microstructures.[21]

In general, to determine which phase will dominate the microstructure after solidification, all the various growth forms must be taken into account. In the present case, Ti dendrites, TiB primary grains and TiB/Ti eutectic must all be considered. The way the interface temperatures of these three growth forms must be considered varies as a function of the solidification rate. The competitive growth criterion has to be applied, i.e., the dominant morphology will be the one having the highest interface temperature for the given growth rate. If the dominant morphology is the eutectic one, then the growth rate of the melt and composition considered are within the "coupled zone" of the alloy.

The alloy is, in fact, of the faceted/nonfaceted type. That is, the TiB phase is a highly anisotropic ceramic material, whereas Ti is a metal. For this reason, the TiB phase has a high entropy of melting and will solidify in highly faceted patterns. The Ti will follow the common solidification behavior of metals and will solidify with the formation of dendrites. The TiB phase will require much higher supercooling (ΔT) for a given growth rate in comparison to Ti dendrites. This effect can be attributed to the change of the diffusion rate of solute away from the dendrite tip as a function of the dendrite geometry (that changes to two dimensional in the case of faceted phases).[21] A description of this behavior is as follows: The difference in the amount of supercooling can be attributed to the higher degree of order that needs to be achieved locally for the nucleation and growth of the highly anisotropic TiB phase in comparison with the more isotropic Ti. This effect also results in a higher amount of supercooling necessary in the case of the nucleation of the eutectic phase as compared with the dendritic Ti; as in the former, TiB is also involved.

A simple function can be used to explain the behavior of this system in a qualitative way. By considering the following two points, the temperature of the interface at solidification varies, T_L^{TiB}, T_L^e, and T_L^{Ti} for the three phases. Each of these temperatures is determined for each B concentration by drawing a line perpendicular to the horizontal axis in the phase diagram. The liquidus temperature of each phase will be the temperature where this line crosses the corresponding liquidus curve (the value for T_L^{Ti} is obtained by extrapolating the liquidus curve up to the relevant B content).

The second point is that at elevated solidification rates, the supercooling necessary for solidification of both eutectic and primary phases is proportional to the solidification rate,[22] but with different proportionality constants depending on which phase is considered (TiB or Ti in the present case).

By taking into account these two points, it is possible to plot for each possible phase a function of the form:

$$T_S = T_L - k \cdot V \quad \text{(Eq 2)}$$

where T_S is the solidification temperature, V is the solidification rate, T_L is the liquidus temperature ($T_L^{TiB} > T_L^e > T_L^{Ti}$), and

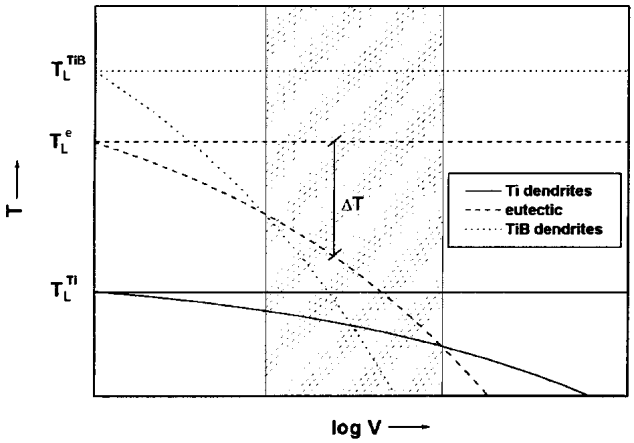

Fig. 8 Solidification temperature as a function of the solidification speed for the three relevant phases. Horizontal lines indicate the normal solidification temperatures and three curves take into account the necessary supercooling (ΔT).

k is a constant relating undercooling to the solidification rate V ($k^{TiB} > k^e > k^{Ti}$). By plotting the various curves, it is possible to determine which phase will exhibit the highest solidification temperature for each solidification rate, and this phase will dominate the final microstructure.

The curves will be typical for each value of atomic percent B, as this changes the liquidus temperatures (T_L). There exists a range of B concentrations and k values for which these curves will have the form depicted in Fig. 8 (where the curves are plotted as a function of log V). The dashed area in Fig. 8 is the "coupled zone," where the eutectic microconstituent dominates the final microstructure. For lower solidification rates, i.e., at the left of the coupled zone in Fig. 8, the primary TiB microconstituent will dominate. For higher solidification rates, the Ti dendrites will dominate. This reasoning applies to the general case where the occurrence of the coupled zone in the alloy is caused by a change in the solidification rate, with the B content being held constant. In the present case, a change in solidification rate is attainable by preheating the substrate, and to a lesser extent, by changing the applied laser power. Both these approaches change the B content of the layers considerably, because they change the melted depth of the melt pool. For this reason, in the present case, the behavior of the system will be slightly more complicated than in the case when only the solidification rate is varied.

Indeed, the atomic B content measured in the coatings varies between 15% and 26%. The values of the liquidus temperature (T_L) for the different phases at these concentrations of B were estimated by choosing k to be 18, 54, and 150 °Cs/mm for Ti, eutectic, and TiB phases, respectively. The solidification rates were not measured during laser cladding. However, they can be roughly estimated to be on the order of laser beam scanning speed (3.3 mm/s). As already mentioned, keeping the solidification rate constant, the TiB will be the phase that needs higher undercooling to solidify; therefore, it will have a higher k value. Titanium will have a much lower value, and the eutectic phase will have a value between them. Besides these conditions, the values for these coefficients are chosen in such a way that all the observed microstructures

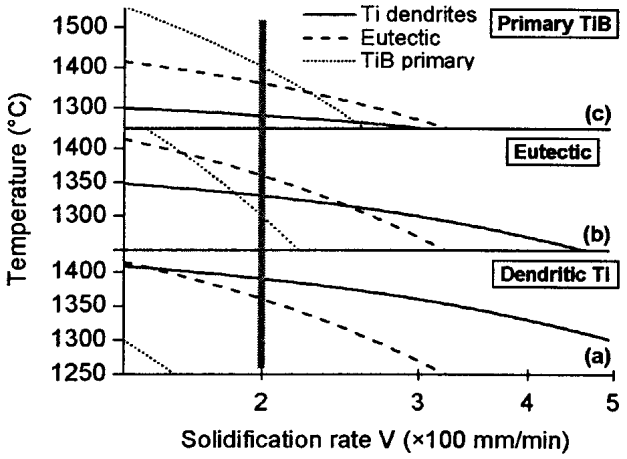

Fig. 9 Solidification temperatures as a function of the solidification speed for the three relevant phases under different atomic boron content in the melt: **(a)** 15%, **(b)** 22%, and **(c)** 26%, which result in the evolution of different microstructures as explained in the text. The gray line highlights the solidification rate at which solidification happened for (b) and (c), whereas for (a) solidification happened at higher values of *V*.

Table 2 Parameters Used for the Curves of Fig. 8

Dominant Microstructure	B Content, at.%	Phases	T_L, °C
Dendritic	15	Ti	1450
	…	Eutectic	1540
	…	TiB	1650
Eutectic	22	Ti	1390
	…	Eutectic	1540
	…	TiB	1800
Primary TiB	26	Ti	1340
	…	Eutectic	1540
	…	TiB	1900

The *k* values are characteristic of each phase. The T_L values change for each phase according to the phase diagram.

might occur with the parameters used in the laser cladding experiments.

According to the parameters listed in Table 2, *T* versus solidification rate have been drawn (Eq 2) for the three microstructures. These diagrams are shown in Fig. 9. Figure 9(a) is related to Fig. 2 (15 at.% B), Fig. 9(b) to Fig. 5 (22 at.% B), and Fig. 9(c) to Fig. 3 (26 at.% B). It can be noticed that the relative position of the curves changes considerably with the variation of B content. Indeed, the relative position of the curves is the key factor in explaining the final microstructure. There is a large portion of Fig. 9(a), where the Ti solidification curve is on top of the other two. It can be inferred that the system was under these conditions of solidification, i.e., somewhere to the right of the gray line in Fig. 9, at solidification rates higher than 200 mm/min. The presence of a eutectic surrounding the Ti dendrites in Fig. 2 is also predicted by inspection of Fig. 9(a). In fact, as solidification proceeds, the temperature shifts to lower values and the growth of the eutectic phase becomes possible, as the eutectic line is crossed.

In the preheated samples, Fig. 9(b) and (c), the solidification rate is lower. The laser power used is higher for the processing conditions in Fig. 9(b), 1400 W, compared with 1000 W for Fig. 9(c), keeping all the other parameters constant. The difference in laser power can hardly cause any change in solidification rate because preheating is applied and Ti has a very low thermal conductivity. Therefore, it can be inferred that the two microstructures solidify at the same rate. If this rate is chosen to be 200 mm/min, the explanation for the resulting microstructures is evident. The system is in the coupled zone for the eutectic system. Lowering the applied laser power enriches the resulting melt in B, and the curve for the TiB solidification temperature shifts upward, because the T_L increases, while the coupled zone is moved more to the right of the graph. The system in this second case will solidify in the normal way, considering that the atomic concentration of B is higher than the eutectic value. TiB primary needles will grow, and subsequently, when the temperature is lower, the system will cross the eutectic line in Fig. 9(c), and the eutectic structure will grow.

By comparing the average value obtained for the hardness of the eutectic layer (7.5 GPa) with the higher and lower bound ROM values (5.4 and 12 GPa, respectively), it can be inferred that the interface is strong enough so that the reinforcement can effectively hinder the deformation of the matrix. Moreover, high-resolution transmission electron microscopy (TEM) on this composite showed that the eutectic TiB needles have a more or less disordered crystallographic structure as compared with the primary ones.[23] This rather disordered structure probably corresponds to a lower hardness, and for the ROM bound calculations, the hardness value measured for the primary needles has been used. Therefore, the real ROM bounds are probably lower, suggesting that the TiB/Ti interface has a higher strength.

The values of wear coefficients measured under the two different loads are remarkably similar considering the microstructure. This fact has two implications. The first is that the different microstructures perform differently in the wear test. The second is that the change of applied stress does not change the wear regimen under which the test is performed. The difference in wear behavior of the coating as a function of its microstructure is very interesting as it confirms what has been observed in the past, i.e., the higher the homogeneity, the higher wear resistance. The enhanced homogeneity of the fully eutectic microstructure has a sensible impact on the performance of the composite layer, which is almost four times better than the primary one (RWR coefficients of about 1500 and 400, respectively).

4. Conclusions

TiB/Ti-6Al-4V MMC clad layers were produced on Ti-6Al-4V substrates by laser treatments. A TiB_2/Ti powder mixture has been used as precursor to obtain a dispersion of TiB needles in the Ti alloy matrix by means of an exothermic reaction between TiB_2 and Ti. Different microstructures were obtained by varying the solidification rate and the atomic percent B in the melt pool. Noteworthy is the result of a fully eutectic microstructure that consisted of an extremely homo-

geneous dispersion of TiB eutectic needles in the Ti alloy matrix, with V_F as high as 0.33. Also, an equilibrium-like microstructure has been obtained consisting of a dispersion of TiB needles, both primary and eutectic, inside the Ti alloy matrix. This microstructure exhibited a high volume fraction of needles, i.e., V_F of 0.4. The hardness and Young's modulus of the primary TiB needles have been measured, $H = 30.7 \pm 1.1$ GPa and $E = 519 \pm 30$ GPa. A hardness profile has been measured also for the eutectic track, yielding an average hardness value of 7.5 GPa, which is considerably higher than the hardness of the base Ti substrate (1.2 GPa). The value for the hardness has been compared with the higher and lower bound values obtained from a ROM calculation. The comparison suggests that the interface between the TiB needles and the matrix is strong. In situ tensile tests also indicated that the interface is strong and resistant to delamination for both the primary and the eutectic needles.

An analysis of the geometry of the layers has been carried out and proved successful in determining the percentage of B, correctly predicting the variation of atomic percent B as a function of the laser power. The high V_F, the hardness improvement, and the quality of the interface between TiB/matrix suggest good performance for the composite during wear. Indeed, this was confirmed by the wear tests. The MMC layers are considerably more wear resistant than the base material, reaching a relative wear resistance as high as 1500.

The fully eutectic microstructure shows the best performance, as its wear resistance is almost a factor of four higher compared with the primary microstructure. The better performance of the fully eutectic microstructure is a consequence of the increased homogeneity of the dispersion of TiB.

Acknowledgment

The Netherlands Institute for Metals Research is acknowledged for its financial support.

References

1. R. Boyer: *Material Properties Handbook: Titanium Alloys,* ASM, Pittsburgh, PA, 1994.
2. Y.T. Pei, V. Ocelik, and J.Th.M. De Hosson: *Acta Mater.,* 2002, *50,* p. 2035.
3. J.A. Vreeling, V. Ocelik, and J.Th.M. De Hosson: *Acta Mater.,* 2002, *50,* p. 4913.
4. J.Th.M. De Hosson and B.J. Kooi: in *Handbook of Surfaces and Interfaces in Materials,* H.S. Nalwa, ed. Academic Press, NY, 2001, Vol. 1, Chap.1, pp. 1-114.
5. E. Zhang, S. Zeng, and B. Wang, *J. Mater. Proc. Technol.,* 2002, *125-126,* pp. 103-09.
6. K.S. Ravi Chandran and K.B. Panda: *Adv. Mater. Proc.,* NY, 2002, pp. 59-62.
7. J.C. Oh, D.-K. Choo, and S. Lee: *Surf Coat. Technol.,* 2000, *127,* pp. 76-85.
8. R. Banerjee, P.C. Collins, and H. L. Fraser: *Adv. Eng. Mater.,* 2002, *4,* pp. 847-51.
9. S. Aich and K.S. Ravi Chandran: *Metall. Mater. Trans. A,* 2002, *33A,* pp. 3489-98.
10. X. Zhang, W. Lu, D. Zhang, and R. Wu: *Scripta Mater.,* 1999, *41,* pp. 39-46.
11. S.C. Tjong and Z.Y. Ma: *Mater. Sci. Eng. R,* 2000, *29,* pp. 49-113.
12. J.A. Vreeling, V. Ocelik, Y.T. Pei, D.T.L. van Agterveld, and J.Th.M. de Hosson: *Acta Mater.,* 2000, *48,* pp. 4225-33.
13. W.C. Oliver and G.M. Pharr: *J. Mater. Res.,* 1992, *7,* p. 1564.
14. I. Barin and O. Knacke, *Thermodynamical Properties of Inorganic Substances,* Springer-Verlag, Berlin, Germany, 1973.
15. Y.P. Lei, H. Murakawa, Y.W. Shi, and X.Y. Li: *Comp. Mater. Sci.,* 2001, *21,* pp. 276-90.
16. R.R. Atri, K.S. Ravichandran, and S.K. Jha: *Mater. Sci. Eng. A,* 1999, *271,* pp. 150-59.
17. S. Gorsse, Y. Le Petitcorps, S. Matar, and F. Rebillat: *Mater. Sci. Eng. A,* 2003, *340,* pp. 80-87.
18. D. Hull, *An Introduction to Composite Materials,* Cambridge University Press, Cambridge, UK, 1981.
19. H.S. Kim, *Mater. Sci. Eng. A,* 2000, *289,* pp. 30-33.
20. I.M. Hutchings, S. Wilson, and A.T. Alpas, in *Comprehensive Composite Materials,* Vol. 3.19, C. Zweben and A. Kelly, ed., Elsevier, Amsterdam, The Netherlands, 2003.
21. H. Biloni and W.J. Boettinger, *Physical Metallurgy,* North Holland, Amsterdam, The Netherlands, 1996, pp. 765-67.
22. W. Kurz and D.J. Fischer, *Fundamentals of Solidification,* Trans Tech Publications LTD, Switzerland, 1986, pp. 97-117.
23. B.J. Kooi, Y.T. Pei, and J.Th.M. De Hosson, *Acta Mater.,* 2003, *51,* pp. 831-45.